Revista Brasileira de Cartografia
ISSN 1808-0936 | https://doi.org/10.14393/revbrascartogr
Sociedade Brasileira de Cartografia, Geodésia, Fotogrametria e Sensoriamento Remoto

Generation of a Digital Terrain Model (DTM) Fusioning WV-2 Images and RTK-derived Topobathymetric Data

Geração de um Modelo Digital de Terreno (MDT) Fusionando Imagens WV-2 e Dados de Topobatimetria Derivados de RTK

Elton Vicente Escobar-Silva [1], Cláudia Maria de Almeida [2], Rômulo Marques-Carvalho [3], João Vitor Roque Guerrero [4] and Cleber Gonzales de Oliveira [5]

[1]Earth Observation and Geoinformatics Division, National Institute for Space Research (INPE), São José dos Campos, Brazil. eltescobar@gmail.com
ORCID: https://orcid.org/0000-0002-9437-9351
[2]Earth Observation and Geoinformatics Division, National Institute for Space Research (INPE), São José dos Campos, Brazil. claudia.almeida@inpe.br
ORCID: https://orcid.org/0000-0002-6523-3169
[3]Earth Observation and Geoinformatics Division, National Institute for Space Research (INPE), São José dos Campos, Brazil. mr.romulomarques@gmail.com
ORCID: https://orcid.org/0000-0002-9232-9043
[4]Institute of Socio-environmental Studies, Federal University of Goiás (UFG), Goiânia, Brazil. jvguerrero2@gmail.com
ORCID: https://orcid.org/0000-0002-5393-3803
[3]VISIONA Space Technology, São José dos Campos, Brazil. cleber.oliveira@ieee.org
ORCID: https://orcid.org/0000-0003-4733-3462

Recebido: 08.2023 | Aceito: 11.2023

Abstract: Digital terrain models (DTMs) are digital elevation models (DEMs) that represent the bare ground surface. They are created by multiple sources, including satellite remote sensing, aerial photography, and ground-based surveys, and are often combined with other data sources to create highly detailed models. As the demand for accurate and detailed information about the Earth's surface continues to grow, DTMs have become an increasingly important tool for researchers in different fields. This study aims to create a DTM with a spatial resolution of 0.50 m for São Caetano do Sul, São Paulo, Brazil, integrated with a topobathymetric map of three water courses running along the borders of the study area. For the conventional DTM generation, a WV-2 stereo pair was used. A total of 55 ground control points (GCPs) were collected using the GNSS-RTK method, being 60% used for model building and 40% employed for validation. The topobathymetric survey was accomplished using a GNSS-RTK device placed along the analyzed open streams. For validation purposes, we used bias and MAE metrics. Overall, the methodology presented in this article provides a useful approach for generating high-resolution DTMs that can be used in a range of applications, especially in urban hydrodynamic studies.
Keywords: Photogrammetry. Bathymetry. Ground control points (GCPs). VHR imagery.

Resumo: Modelos digitais de terreno (MDTs) são modelos digitais de elevação (MDEs) que representam a superfície do solo. Eles são criados por diversas fontes de dados, incluindo sensoriamento remoto por satélite, fotografia aérea e levantamentos terrestres, e geralmente são combinados com outras fontes de dados para criar modelos altamente detalhados. À medida que a demanda por informações precisas e detalhadas sobre a superfície da Terra continua a crescer, os MDTs tornaram-se uma ferramenta cada vez mais importante para pesquisadores em diferentes campos. Este estudo visa criar um MDT com resolução espacial de 0,50 m para São Caetano do Sul, São Paulo, Brasil, integrado a um mapa topobatimétrico de três cursos d'água que correm ao longo dos limites da área de estudo. Para a geração DTM convencional, foi usado um par estéreo WV-2. Um total de 55 pontos de controle de solo (GCPs) foram coletados usando o método GNSS-RTK, sendo 60% utilizados para construção do modelo e 40% empregados para a sua validação. O levantamento topobatimétrico foi realizado utilizando um dispositivo GNSS-RTK colocado ao longo dos riachos abertos analisados. Para fins de validação, foi utilizado métricas de viés (bias) e erro absoluto médio (MAE). No geral, a metodologia apresentada neste artigo fornece uma abordagem útil para gerar MDTs de alta resolução, que podem ser utilizados em uma variedade de aplicações, sobretudo em estudos hidrodinâmicos urbanos.
Palavras-chave: Fotogrametria. Batimetria. Pontos de controle de solo (GCPs). Imagens VHR.

1 INTRODUCTION

A digital elevation model (DEM) is an umbrella term for any electronically accessible elevation datasets. It contains elevation measures of any object on Earth's terrain (bare-earth, transmission towers, viaducts, vegetation canopy, water bodies, etc.) according to a given vertical datum (MAUNE et al., 2018). Hereinafter, a digital surface model (DSM) represents the earth's surface and includes all objects on it, such as buildings and vegetation. On the other hand, a digital terrain model (DTM) denotes the bare ground surface without any objects on it (GUTH et al., 2021). For the purpose of standardizing the terms in this work and easing its comprehension, DEM will be used as term that encompasses both DSM and DTM.

The elevation data required to create a DEM can be collected from different approaches, such as ground surveys, digitization and interpolation of contours in existing hardcopy topographic maps, and remote sensing (RS) techniques. Some of the most popular methods using RS techniques include kinematic global navigation satellite system surveys, stereo-photogrammetry, synthetic aperture radar (SAR) interferometry, aerial or airborne laser scanning, and fusion of data from different sources (FU; TSAY, 2016). However, as any spatial dataset, DEMs are subject to different types of errors (FISHER; TATE, 2006; WECHSLER; KROLL, 2006). The most common errors can be grouped into three categories: (i) gross error during data collection (RODRÍGUEZ et al., 2006); (ii) deficient orientation of stereo images (HUISING; GOMES PEREIRA, 1998); and (iii) grid spacing and interpolation techniques (FISHER; TATE, 2006; FU; TSAY, 2016).

So far, the first released and most known free source of elevation data at a nearly global scale has been provided by NASA's Shuttle Radar Topography Mission (SRTM). The data were acquired in early 2000 and since then several versions of SRTM have been released, with the most recent version data set (30 m resolution) released in late 2015 (NASA, 2022). However, since the data were acquired over 20 years ago, they are out of date. Furthermore, SRTM is known to contain large errors with a positive bias (SHORTRIDGE, 2006), especially in vegetation (e.g., ORLANDI et al., 2019; WEYDAHL et al., 2007) and urban areas (e.g., GAMBA et al., 2002; LIU et al., 2021).

Errors are undesirable in DEM once they can be propagated to DEM-derived products (e.g., aspect, slope, hillshade, and surface curvature among others). DEMs errors occur in both the horizontal and vertical directions (FISHER; TATE, 2006). As an example of the consequences of these errors, considering flood-risk analyses, a small error in a DEM, especially in a flood-prone area, results in a significant change in the flood-risk map of such area (ZAZO et al., 2015), especially in urban areas (FEWTRELL et al., 2011). Therefore, it is expected that DEMs have sufficient quality to meet the needs of their applications.

A quantitative representation of the Earth's surface provides basic information about terrain relief. However, accurate estimates of DEMs are of fundamental importance for regional and local-scale analysis in diverse areas, such as hydrology, environmental modeling, urban planning, and geology (CRONEBORG et al., 2020). In this context, the production of high-quality DEMs has significantly benefited from advances in RS techniques over the past decades (MESA-MINGORANCE; ARIZA-LÓPEZ, 2020). As very high-resolution (VHR) satellite imagery (e.g., WordView, IKONOS, QuickBird, Pleiades, and GeoEye) have become available for commercial use, the stereo images from such space imaging systems have been used to generate high-quality DEMs (e.g., SHAKER et al., 2010; ZHOU et al., 2015). However, to achieve such quality, the users must be aware of the costs of the products, though. In parallel with this, the global navigation satellite system (GNSS) positioning method with real-time kinematic (RTK) correction represents a milestone in the accurate determination of elevation. This approach can improve the accuracy from meters to a few centimeters (TEUNISSEN et al., 2014). However, to ensure reliable and high accurate results (e.g., 2-cm root mean square error – RMSE), it is required that the roving receiver is located within a restricted range (up to 15 km) of the reference station (CINTRA et al., 2011). Furthermore, the ground controls points (GCPs) collected by GNSS-RTK surveying are usually used for DEMs calibration and validation.

In this context, bathymetry is the study of the beds or floors of water bodies, such as oceans, rivers, streams, and lakes (WÖLFL et al., 2019). In the same way that topographic maps represent the three-dimensional features (or relief) of overland terrain, topobathymetric maps illustrate the underwater depth of

water bodies as well as submerged relief (WEATHERALL et al., 2015). Therefore, accurate bathymetry plays a key role in a variety of hydrologic and hydraulic applications (e.g., flood modeling).

Given the foregoing, this work aims to produce a DTM with a spatial resolution of 0.5 m generated from a stereo-pair WorldView-2 (WV-2) images and merged with a topobathymetric map resulting from a GNSS-RTK survey accomplished for three streams running along the borders of the study area. We reported the procedure for generating the DTM as well as evaluated its accuracy. For this purpose, GCPs were collected in a field survey and used both in the DTM generation and validation. Furthermore, the DTM generated in this work was also compared with a 5-m spatial resolution DTM derived from aerial digital photos. Lastly, we believe that (i) the result of this work will support future evaluations of digital terrain models (DTMs) generated for urban areas relying on satellite imagery; and (ii) the coupling between a DTM and a topobathymetric map of water streams is crucial for urban hydraulic studies, as it is the case of flood risk assessment and management.

2 MATERIAL AND METHODS

2.1 Study area

The study site is the municipality of São Caetano do Sul, which is located in the southern São Paulo Metropolitan Area (Figure 1). São Caetano do Sul belongs to an important economic region in Brazil, named ABCD Region. The municipality is intensely conurbated with the municipalities of São Paulo, Santo André, and São Bernardo do Campo, with visually undefined boundaries among them. According to the Brazilian Institute of Geography and Statistics, the current population of São Caetano do Sul is estimated at about 162,763 inhabitants in an area of 15.33 km^2 (IBGE, 2023). São Caetano do Sul is the second city with the highest economic density (GDP/km^2) in the country (IBGE, 2020) and according to the United Nations Sustainable Development Goals, the municipality holds the 1st position in the ranking of sustainable cities in Brazil (ICS, 2022).

Figure 1 – Images showing the location of São Caetano do Sul, São Paulo, Brazil. (A) Location of São Paulo State in Brazil; (B) Location of São Caetano do Sul in São Paulo State; (C) Buffer of 500 m surrounding the municipal boundaries of São Caetano do Sul.

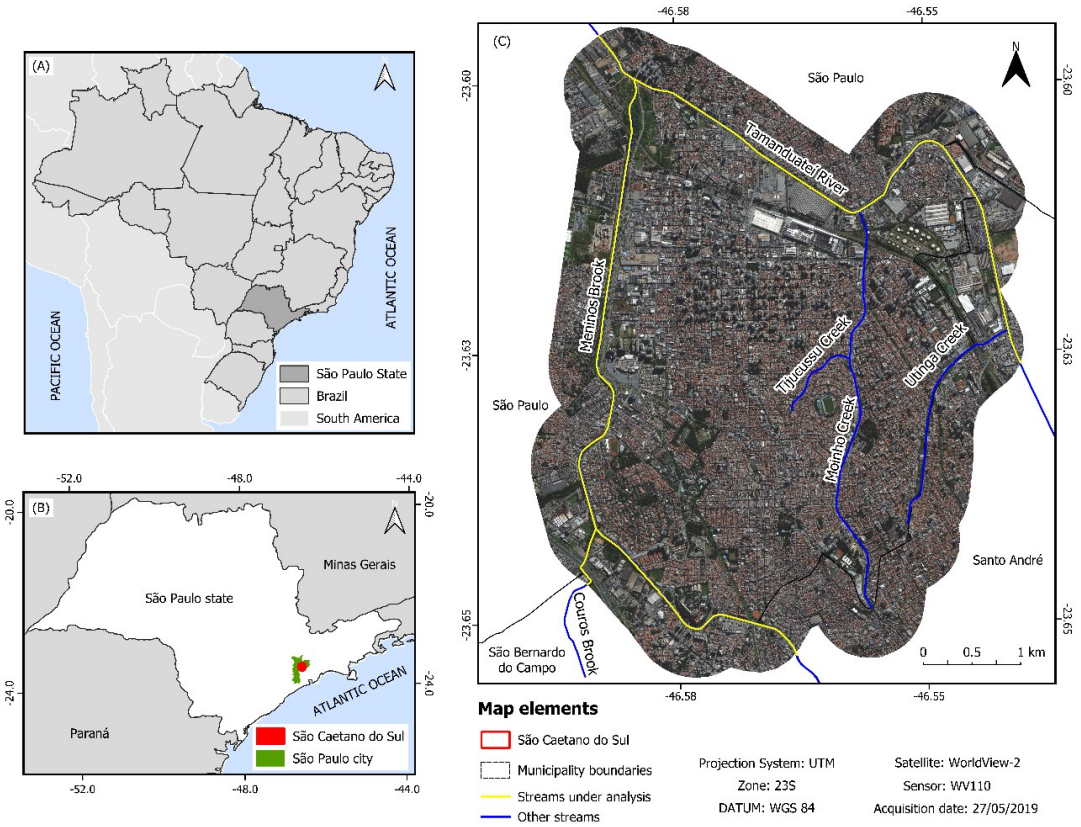

Elaboration: The authors (2023).

São Caetano do Sul is situated on a plateau adjacent to the Serra do Mar (Portuguese term for *"Sea Range"*). According to Köppen's climate classification (BECK et al., 2018), São Caetano do Sul presents a humid subtropical climate, with a mildly warm and rainy summer, and a moderate and dry winter. The average annual temperature is about 19.5° C, and the coldest and warmest months are respectively July (average of 16.2 °C) and February (average of 22.5 °C) (CLIMATE-DATA.ORG, 2023). The annual rainfall is around 1,496 mm. The 30-year average annual rainfall was generated from Stream Gauge Station No. 2346051 of the Department of Water and Electricity (Departamento de Águas e Energia Elétrica – DAEE) of São Paulo State.

2.2 Satellite images

WV-2 spacecraft was launched in 2009 and has an expected lifespan of 13 years due to some improvements (its initial expected lifespan was nearly 7.5 years). The WV-2 satellite sensor comprises a high-resolution panchromatic band and 8 (eight) multispectral bands (coastal, blue, green, yellow, red, red-edge, near-infrared 1, and near-infrared 2). More specifically, WV-2 provides 0.5 m panchromatic resolution and 2 m multispectral resolution images with 11 bits of radiometric resolution per pixel. The satellite has an average revisit time of approximately 1.1 days, and it is capable of collecting nearly 1 million km^2 of Earth surface images per day. WV-2 operates at an altitude of 770 km in a sun-synchronous orbit with a period of 100 minutes (ESA, 2022).

Due to the unavailability of recent stereo-pair imagery without clouds over São Caetano do Sul, we opted for using two WV-2 images collected on different dates. The VHR images were collected on 27/05/2019 and 15/07/2019 (difference of 49 days between the acquisition dates), with image off-nadir angles of 21.5° and 15.7°, respectively (Supplementary Table 1). It is important to highlight that these two images were used in the DTM generation process since it is assumed that consolidated urban landscapes tend to change little in a short period, such as the city of São Caetano do Sul (CARVALHO et al., 2022). Finally, aiming to avoid undesirable edge effects during image processing procedures, a buffer of 500 m surrounding the official municipality boundaries was adopted to define the image sizes (Figure 1C). Thus, each image has an area of approximately 25 km^2.

2.3 Collection of GCPs with RTK positioning

In this work, a GTRi geodetic receiver was used. GTRi is a fully integrated GNSS receiver, compatible with other equipments. It is capable of sending SMS messages in real-time indicating battery level, signal quality, and positioning. It has an internal 400 MHz UHF radio with transmitting and receiving capability, which eliminates the need for cables in the base and rover configuration.

The field campaign was performed on April 28 and 29, May 2 and 3, and October 11 of 2022. The study area was divided into 28 identical quadrants with about 1.03 km^2. It is worth mentioning that we sought to collect at least 1 point within each quadrant, aiming thus at a homogeneous spatial distribution of points. The datum World Geodetic System 1984 (WGS 84) was used as the spatial reference frame. Since the study area is located in a highly urbanized region and with a high concentration of buildings, 8 base stations were needed to perform this work. We sought to collect ground points that could be visibly identified in the 0.50 meter-resolution image (only pure pixels were selected in this work). Overall, 55 GCPs were collected during the five surveying days (Supplementary Table 2 and Supplementary Figures 1 and 2). Lastly, elevation data were automatically referenced by geoidal hgeoHNor2020 model to mean sea level of Imbituba Brazilian Vertical Datum, located in the southern state of Santa Catarina.

2.4 DTM generation

To extract height information from the stereo-pair and hence generate a DSM and DTM, we used the OrthoEngine module within CATALYST software, a PCI Geomatics brand. It is important to highlight that only panchromatic images were used in the DTM generation. The math modeling method used for the DEM

generation was the rational function (RF) model, which is recommended when the user does not dispose of the whole image, which is our case (we only have a clipping of the full scene) (PCI GEOMATICS, 2022). Basically, RF is a simple mathematical model that builds a correlation between the pixels and their ground locations. The projection of the output images and GCPs were set in meters using WGS 84 as the horizontal reference datum.

The study area is located in UTM Zone 23 K. The output pixel spacing was defined as 0.50 m (the same as the WV-2 images resolution), the elevation was set in meters, and the elevation reference chosen was the mean sea level (MSL). In the processing step, 22 tie points (TPs) (Supplementary Figures 3) were additionally collected in the images, associated with homologous features at the ground level and with no elevation information. For validation purposes, from the 55 GCPs collected, 33 points (60%) were used for building the mathematical model used in the DEM generation and 22 points (40%) were especially reserved for the validation procedure as independent check points (ICPs) (Supplementary Table 2 and Supplementary Figure 2). Lastly, the horizontal bias and their respective standard deviation (std. dev.) of the 33 GCPs used for the DEM generation were less than 0.5 m for both images, a sub-pixel value (for detailed information see Supplementary Material).

OrthoEngine uses image correlation to extract matching pixels in the two images and then uses the sensor geometry from the computed math model to calculate x, y, and z positions of the DEM. Creating epipolar images increases the speed of the correlation process and reduces the possibility of incorrect matches (PCI GEOMATICS, 2022). In the epipolar image creation step, the maximum overlapping pairs algorithm was used. This algorithm automatically selects which image will be on the left and on the right side. A minimum percentage overlap of 50% was set. The downsample factor was selected to be 1:1, i.e., to preserve the same pixel size of the images (0.50 m). As a result, the parallax images (or epipolar pair) are generated.

The next step is the DSM generation. For the extraction method, semi-global matching (SGM) was selected. SGM produces higher resolution results with fewer errors and higher detailing. However, it is necessary a longer processing time compared to the normalized cross-correlation (NCC) method (PCI GEOMATICS, 2022). Aiming to obtain the best possible result, SGM extraction method was chosen. Then, the following settings were adopted: (i) output DSM vertical datum: MSL; (ii) pixel sample interval: 1 (i.e., the same as the input images); (iii) smoothing filter: high; (iv) clean up building edges with filter size: 31. The DEM generation already included geocoding, and the pixel resolution of it was defined as 0.50 m. It is important to mention that all these parameters were defined after manifold trials (the best visual result was chosen and applied in this work).

In CATALYST, there are two primary tools to convert a DSM into a DTM: (i) a DEM editing tool and (ii) the DSM2DTM algorithm. The DEM editing tool provides a manual method of conversion from DSM to DTM that allows for very fine control of the conversion process. On the other hand, the DSM2DTM algorithm is an automated process (PCI GEOMATICS, 2022). Seeking to obtain the finest result as possible, we used the DEM editing tool to convert the DSM into a DTM. The following order of filters was applied: (i) terrain (five successive times – detailed below) and (ii) fill from edges.

As terrain filters, we used the flat option (the most appropriate for our study area). There are two main parameters within the terrain filters which can be set by the user: size and gradient. Size is measured in pixels; therefore, the user must convert the desired size in meters to pixels when entering the value. For removing buildings that are 100 m in diameter, the user needs to calculate: 100 (size in meters) / 0.50 (image resolution in meters) = 200 (size in pixels). Typically, it is best to set this value to the size of the largest building found in the scene. Gradient is measured in degrees, ranging from 0° to 90° (from completely flat to completely vertical). This is a key parameter, as it defines the cutoff range for objects to remain in the DTM. For example, specifying 30° will cause the filter to remove everything from the terrain that exceeds 30° degrees in slope, as long as it is also within the specified size (PCI GEOMATICS, 2022). For size and gradient, we applied the following terrain filters sequence: (i) size = 2,000 pixels and gradient = 30°; (ii) size = 1,500 pixels and gradient = 25°; (iii) size = 1,000 pixels and gradient = 20°; (iv) size = 500 pixels and gradient = 15°; and (v) size = 100 pixels and gradient = 10°. Lastly, manual touch-up edits were applied using the fill from edges filter to remove buildings leftovers or clean up roads along their edges as well as fill in spurious holes in the terrain.

2.5 Topobathymetric map generation

The field campaign was performed from August 29 to September 19 of 2022. The GNSS receiver used in this work was the GeoMax Zenith 35 Pro (GeoMax, Widnau, Switzerland) with a Samsung datalogger using XPAD Field software. The Zenith 35 Pro supports 555 channels (multi-constellation) and multi-frequency, and it can connect up to 10 rovers simultaneously. The GNSS receiver using RTK can provide a precision of 1.5 cm for axes x and y, and 2 cm for axis z (www.geomax-positioning.com).

Three stretches of the Tamanduateí River (Rio Tamanduateí) and Meninos Brook (Ribeirão dos Meninos) were mapped, which compose the territorial boundary of the municipality of São Caetano do Sul, and also a small stretch of Couros Brook (Ribeirão dos Couros) that flows into Meninos Brook (Figure 1C – streams under analysis). An extension of 15.41 km was surveyed along them. The fieldwork for collecting ground points consisted in the following strategies: (i) the depth of the middle of the watercourse was surveyed every 50 m; and (ii) the cross-section of the watercourse (one point on each bank of the stream and one point in the middle of the watercourse) was surveyed every 200 m. However, due to the fact that some depths surpassed the surveyor's height, 15 center points could not be surveyed. In such cases, an average between the immediately preceding and succeeding points was estimated. Overall, 462 points were collected along the three reaches. As previously mentioned, elevation data are referenced to mean sea level of Imbituba Brazilian Vertical Datum, located in the state of Santa Catarina. A private fixed station located 11 km away from our study area was employed as a reference for converting ellipsoidal into orthometric heights.

It is important to highlight that control points were collected with the purpose of helping draw the bounding polygon of the study area. These points were collected in stretches with peculiar features, such as curves or flood control structures. There are some retention ponds along the stretch of the Meninos Book (Supplementary Figure 4). Detention ponds are used to temporarily catch and hold stormwater but remain mostly dry. They are designed as a backup to municipal drainage systems during big storms to prevent flooding and erosion of local streams and lakes.

Regarding data processing, midpoints were created between the collected points aiming to improve data interpolation, i.e., to avoid calculation errors in the interpolation procedure. The average value of altitudes between the previous and posterior points was assumed for midpoints. Thus, the interval between points was reduced to 25 m. Next, a polygon covering the entire area of the three reaches of the water streams was created from the points on the banks of the surveyed cross-sections and the control points. This polygon was used as a mask for creating the topobathymetric map of the study area. To do so, we used the tool *'point to path'* in QGIS 3.22, a free and open-source cross-platform desktop geographic information system application. Then, the topobathymetric map was created using the triangulated irregular network (TIN) interpolation in QGIS, adopting the linear method in this procedure. The output cell size was set to 0.5 m.

2.6 Combining the DTM and the topobathymetric map

The final product of this work is a raster file with a spatial resolution of 0.50 m resulting from the merging of the DTM (Section 2.4) and the topobathymetric model (Section 2.5). For this, we used the QGIS merge tool. It is important to note that this tool allows one to combine more than one raster to generate a single product, provided that all raster layers are in the same coordinate system.

2.7 Validation and accuracy assessment

In CATALYST, a total of 22 points (40%) set as ICPs were used in the validation procedure (Supplementary Table 2). The sample size above 20 points was defined according to the standards for DEM by the United States Geological Survey (USGS, 1986). The points were chosen aiming to cover as much of the image as possible, avoiding the borders though (Supplementary Figure 2).

Before choosing the statistical metrics to be adopted, it becomes necessary to apply a normality test to the elevation data. To do so, we employed the Shapiro-Wilk test (VILLASENOR ALVA; ESTRADA, 2009), in which p-values equal to or greater than 0.05 indicate a normal distribution. The result of the Shapiro-Wilk

test using the GCPs elevation data showed a *p*-value equal to 2.56×10^{-6} (Supplementary Material, Section 3), revealing the non-normality nature of our data.

According to Seegers et al. (2018), commonly used statistical methods based on mean squared errors, such as the coefficient of determination (r^2), RMSE, and regression slopes, are most appropriate for Gaussian distributions without outliers. On the other hand, metrics based on simple deviations, such as bias and mean absolute error (MAE), as well as pair-wise comparisons, often provide more robust and straightforward quantities for evaluating model-performance error with non-Gaussian distributions and outliers (SEEGERS et al., 2018). Therefore, we applied bias and MAE statistics for the validation and accuracy assessment of the DTM generated within CATALYST. In the case of the topobathymetric survey, since all collected points were used to build the map, the topobathymetric validation could not be performed.

Bias (systematic error) offers a simple description of the systematic direction of the error, as either over- or under- estimating the prediction on average. On the other hand, MAE is the mean of the total absolute difference between the true and predicted value (WALTHER; MOORE, 2005). These metrics can be obtained as follows (Eq.1 and Eq. 2):

$$bias = \frac{\sum_{i=1}^{n}(M_i - O_i)}{n} \quad (1)$$

$$MAE = \frac{\sum_{i=1}^{n}|M_i - O_i|}{n} \quad (2)$$

where M, O, and n represent the modeled value, the observation, and the sample size, respectively.

Furthermore, the DTM generated in this work will be compared with the DTM (5 m of spatial resolution) generated by the São Paulo Metropolitan Planning Company SA (Empresa Paulista de Planejamento Metropolitano SA – EMPLASA) (Supplementary Figure 5). EMPLASA DTM was generated from aerial photographs acquired between 2010 and 2011 (ROMANHOLI et al., 2015). The employed photogrammetric technique extracted three-dimensional coordinates, using correlation in one or more photographic pairs, generated automatically by automatic terrain extraction (MUGNIER et al., 2013). This comparison between the DTMs includes (i) the statistics (bias and MAE) of the elevation points generated by CATALYST and EMPLASA compared to the GCPs collected with GNSS-RTK (true values), and (ii) a topographic profile of a transect crossing the study area in the W–E direction. Both the GCPs values and the topographic profile were obtained using QGIS.

3 RESULTS AND DISCUSSION

The DTM with a spatial resolution of 0.50 m is shown in Figure 2. For illustrative purposes, a 3D visualization of the topobathymetric map is shown in Supplementary Figure 6. The elevation ranged from 722.83 m to 811.97 m above sea level. The highest elevations are concentrated in the central and southeastern parts of the study area. On the other hand, the lowest elevations are situated in the northwestern region, near the confluence of Meninos Brook and Tamanduateí River. The mean elevation is about 757.62 m. The spatial distribution of the 22 GCPs used as ICPs in the validation procedure is also shown in Figure 2.

 DOI: http://dx.doi.org/10.14393/rbcv76n0a-70372

Figure 2 – Digital terrain model (DTM) of São Caetano do Sul (SP) with a spatial resolution of 0.50 m. (A) Zoom into the detention pond structures within Meninos Brook; (B) Spatial distribution of the 22 GCPs used as ICPs.

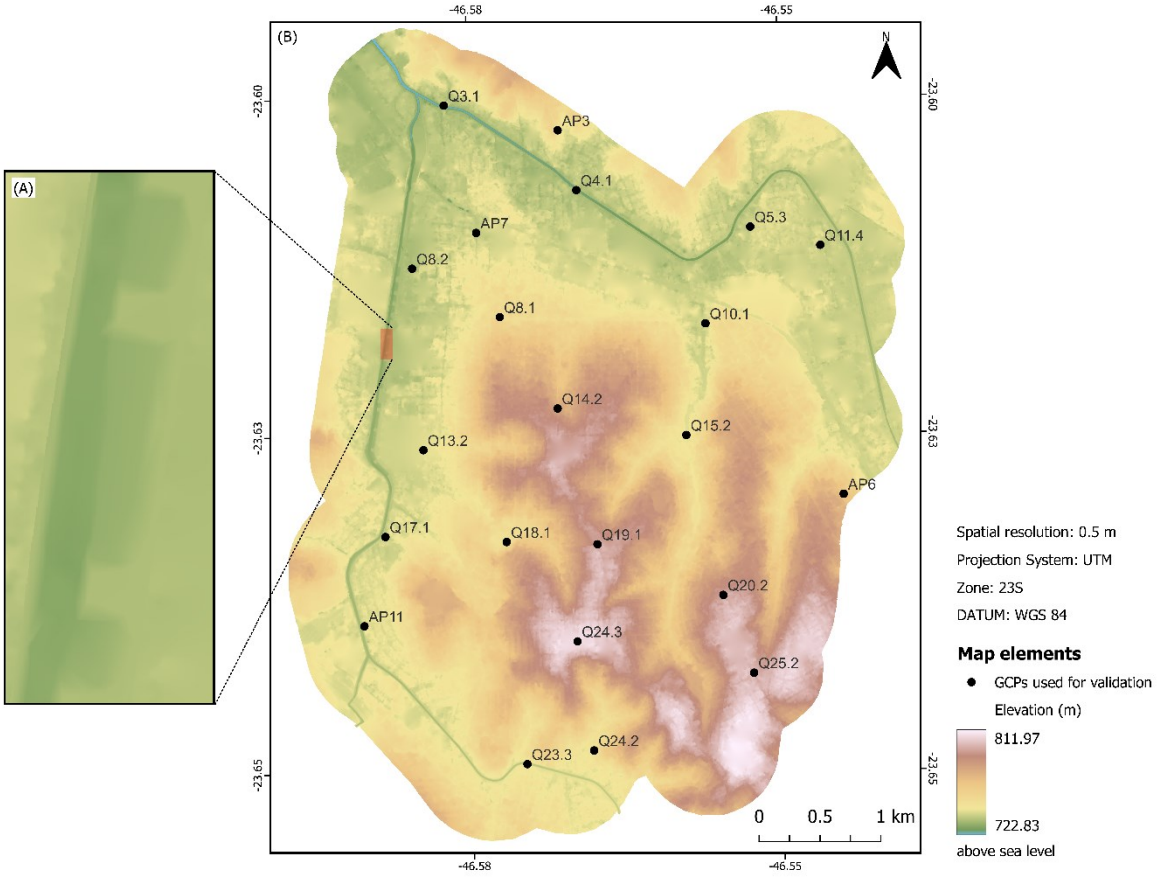

Elaboration: The authors (2023).

Table 1 shows the errors and the absolute errors between the modeled GCPs and the observed GCPs (in this case, the GNSS-RTK points) for both DTMs (with 0.50 m and 5 m of spatial resolution). Considering the DTM with 0.50 m of spatial resolution (the product of this work), the errors between its modeled (M_i) and observed points (O_i) ranged from -0.02 to 1.82 m, with a median of 0.42 m and a bias (or mean) of 0.67 m. The standard deviation is 0.58 m, and the MAE is 0.67 m (Table 2). On the other hand, considering the EMPLASA DTM, the errors between the modeled (M_i) and observed points (O_i) ranged from -4.72 to 1.01 m, with a median of 0.44 m and a bias (or mean) of -0.04 m. Its standard deviation is 1.44 m, and the MAE is 0.88 m (Table 2). A box plot showing the bias of both DTMs is presented in Figure 3. Considering that the bias shows the errors directions (over or under-estimating them) and the MAE accounts for the mean of the total absolute difference between the observed and modeled values, we can claim that the DTM generated in this work presents better accuracy as compared with the EMPLASA DTM (over 31%).

Table 1 – Elevation of the GCPs used as ICPs collected by GNSS-RTK and the respective points generated in the DTMs with 0.5 and 5 m of spatial resolution. The errors and absolute errors between the modeled and observed points for both DTMs are also presented. *Q3 means Quadrant number 3 (three); dot(.) is used to separate the quadrant number and the respective ground control point number inside it; and AP means additional point.

ID*	ICPs elevation (m)	CATALYST DTM (0.5 m)		EMPLASA DTM (5 m)	
		elevation (m)	$M_i - O_i$	elevation (m)	$M_i - O_i$
Q3.1	733.18	733.29	0.11	729.56	-3.62
Q4.1	734.83	735.63	0.80	730.11	-4.72
Q5.3	737.54	737.61	0.07	738.03	0.49
Q8.1	751.1	751.47	0.37	751.6	0.50
Q8.2	734.64	735.10	0.46	735.61	0.97
Q10.1	739.55	740.66	1.11	740.16	0.61
Q11.4	737.58	737.73	0.15	738.02	0.44
Q13.2	741.25	743.07	1.82	741.65	0.40
Q14.2	776.04	776.42	0.38	776.21	0.17
Q15.2	743.28	743.54	0.26	743.69	0.41
Q17.1	738.21	738.85	0.64	738.3	0.09
Q18.1	748.12	749.71	1.59	748.57	0.45
Q19.1	794.04	794.16	0.12	794.25	0.21
Q20.2	789.49	789.80	0.31	790.4	0.91
Q23.3	742.93	743.19	0.26	741.57	-1.36
Q24.2	743.62	745.35	1.73	744.19	0.57
Q24.3	805.9	806.98	1.08	805.51	-0.39
Q25.2	795.31	795.85	0.54	796.32	1.01
AP3	748.45	748.76	0.31	748.97	0.52
AP6	765.98	765.96	-0.02	766.14	0.16
AP7	736.25	737.75	1.50	736.78	0.53
AP11	737.91	739.04	1.13	738.75	0.84

Elaboration: The authors (2023).

Table 2 – Statistics of the comparison between the DTM generated in this work (0.50 m) and the EMPLASA DTM (5 m).

	DTM 0.50 m	DTM 5 m
minimum	-0.02	-4.72
maximum	1.82	1.01
median	0.42	0.44
bias (mean)	0.67	-0.04
MAE	0.67	0.88
Standard deviation	0.58	1.44

Elaboration: The authors (2023).

 DOI: http://dx.doi.org/10.14393/rbcv76n0a-70372

Figure 3 – Box plot indicating the bias of both DTMs. Q1, Q2 and Q3 mean respectively lower quartile (25%), middle quartile (median), upper quartile (75%).

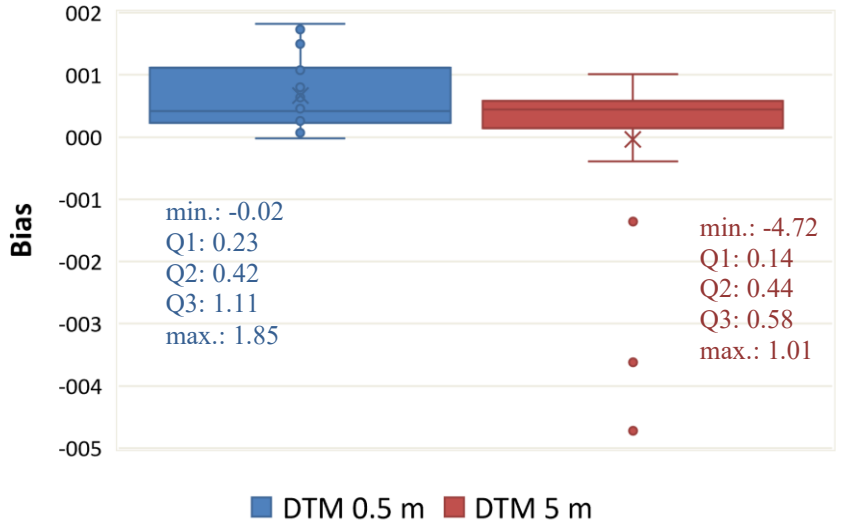

Elaboration: The authors (2023).

Considering the pixel size of the WV-2 image (0.50 m) as a threshold, 10 modeled points in CATALYST presented errors higher than 0.50 m (Q4.1, Q10.1, Q13.2, Q17.1, Q18.1, Q24.2, Q24.3, Q25.2, AP7, and AP11). The EMPLASA DTM in turn presented 11 points with errors above this threshold. Seven (7) points were wrongly estimated in both DTMs (Q4.1, Q10.1, Q13.2, Q24.2, Q25.2, AP7, and AP11), which may suggest a common simulation error for these areas. Despite a small difference in the number of erroneously modeled points (10 points in the DTM with 0.50 m; 11 points in the DTM with 5 m), EMPLASA DTM presented a greater amplitude in errors (underestimated values), which may be related to the degradation of the spatial resolution of the DTM (i.e., a spatial resolution of 5 m is 100 times less detailed than a DTM with 0.50 m of spatial resolution).

NOVOA et al. (2015) evaluated, at the agricultural plot scale, the possibilities and limitations of a WorldView-2 (WV-2) DEM for representing elevation and their finding showed an overall vertical accuracy of 0.45 m. Nemmaoui et al. (2019) created a high-quality DSM and DTM from WorldView-2 along-track stereo pair meant to obtain 3D geospatial features. DSM yielded vertical accuracy results with mean errors ranging from 0.01 to 0.35 m and random errors (standard deviation) between 0.56 and 0.82 m, while DTM showed mean errors between 0.27 and 1.78 m and random errors ranging from 1.16 to 2.28 m. Lastly, Aguilar et al. (2019) explored the capabilities of VHR satellite stereo pairs for DSMs generation over different land-cover objects. Their DSM statistics showed random errors between 0.22 and 1.53 m.

Figure 4 shows a horizontal topographic profile (see Supplementary Figure 7 to see the location of this topographic transect in the study area). The DTM with 0.50 m showed higher elevation values compared with the EMPLASA DTM, as shown by the validation results. It can be observed sudden changes in the elevation values within the DTM with 0.50 m (red circles in Figure 5), which are not noticed in the EMPLASA DTM. This change in elevation values is related to the finer resolution of the DTM with 0.50 m. In general, both DTMs present similar patterns in the elevation values distribution along the analyzed topographic profile.

Figure 4 – Vertical topographic profile of a transect across the W–E direction (see Supplementary Figure 7 to see the location of the topographic profile in the study area). Red circles highlight sudden changes in the terrain elevation.

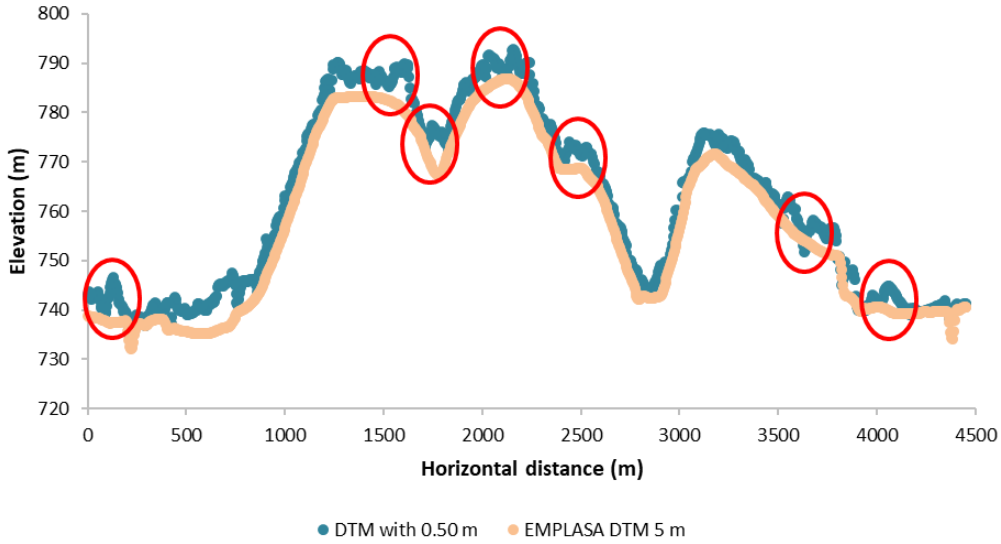

Elaboration: The authors (2023).

The presence of noise in the DSM and DTM generated by the WV-2 stereo pair images could be explained by two reasons: (i) for better results with the SGM algorithm, it is recommended an intersection angle of image acquisition between 5° – 45°; images with lower intersection angles (0.7° as in the case of this work) may present similar geometric configurations and unfavorably impact the stereo pair byproducts (QIN, 2019); (ii) a very-high resolution DTM (as a DTM with spatial resolution of 0.50m) carries the interference of a lot of features (buildings, threes, automobiles, etc.) from the stereopair image. As a result, the DTM presents greater variation in the elevation of the relief compared to DTM with lower spatial resolution. In other words, coarser DTMs present more homogeneous relief and smoothed changes in the slope (HENGL; EVANS, 2009; GROHMANN, 2015).

The elevations in the reaches of the analyzed streams ranged from 722.91 to 740.20 m. The lowest elevation value was observed in the lower Tamanduateí River (close to the confluence of Meninos Brook), located in São Paulo city. On the other hand, the highest elevation value was found in the upper Meninos Brook (close to the confluence of Couros Brook), located in São Bernardo do Campo. Figure 2A highlights detention pond structures in Meninos Brook, which could only be modeled due to strategic control points collected during the fieldwork. The mapping of such structures provides accurate data crucial for flood simulation experiments.

As well as almost all urban rivers in Brazil, the analyzed reaches have been subjected to a rectification process, i.e., the water streams lost the original form of their courses. Since urban rivers have long straight distances and few curves, we believe that few details of the watercourse forms were lost (probably minor sections in the curved stretches). In this context, the methodology adopted in this work for the collection of topobathymetric sample points seemed to be appropriate for its purpose. However, shorter distances (<50 m) should be used in curved stretches.

An important aspect to be highlighted is the presence of several silted stretches in the three analyzed water courses. This silting is due to sediments as well as debris from construction and garbage. As a result, the watercourse channel is drastically reduced in these stretches, and it is thus recommended that the collection interval of the topobathymetric sample points be less than 200 m along them. In fact, a maximum distance of 100 m is highly recommended.

4 CONCLUSION

This work sought to generate a DTM with 0.50 m of spatial resolution for São Caetano do Sul, São Paulo, Brazil, integrated with a topobathymetric survey meant for the streambeds modeling of three water courses running along the city borders. For the conventional DTM generation, a WV-2 stereo pair of the study area was used. A total of 55 GCPs were collected using the GNSS-RTK method, of which 33 points (60%)

were used for model building, while 22 points (40%) were employed for validation. CATALYST® software was used to generate the DSM and subsequently the DTM. For validation purposes, we used bias and MAE metrics, as suggested by Seegers et al. 2018) in view of the non-normality nature of our data.

The errors between the estimated DTM (with 0.50 m of spatial resolution) and collected points ranged from -0.02 to 1.82 m, with a positive bias and MAE of 0.67 m. The values of MAE above 0.50 m may be related to the low intersection angle between the two stereo pair images (Supplementary Table 1) according to Qin (2019). Furthermore, it can also be related to the fact that the images were collected on different days, having a snapshot of the traffic at different times, i.e., the arrangement of the vehicles can cause confusion in the model building. Compared with EMPLASA DTM, our results showed better accuracy (over 31%).

Regarding the topobathymetric map, although the higher precision and accuracy of the field surveying method, such procedure also relies on the surveyors' abilities to achieve satisfactory results. Thus, following a protocol previously defined for field data collection is essential to obtain reliable data. Furthermore, the mapping of the detention ponds is critical in cases where the topobathymetric map will be further employed, as in flood simulation experiments. In order to acquire a better detail of the watercourse shape, it is recommended, whenever possible, to collect bathymetric sample points at intervals less than 50 m in curved stretches, and cross sections at intervals of 100 m or less. And finally, we ought to mention that the product generated in this work is expected to provide VHR input data for urban flood modeling studies.

Acknowledgments

This study was funded by the São Paulo Research Foundation (FAPESP), grants 2021/11435-4 (E.V.E.S.) and 2020/09215-3 (C.M.A.), the Brazilian National Council for Scientific and Technological Development CNPq, grants 311324/2021-5 (C.M.A.) and 130599/2022-0 (R.M.C.), and the Brazilian Coordination for the Upgrade of Graduate Personnel CAPES, Finance Code 001 (E.V.E.S.). We thank MAXAR for providing the WV-2 images for academic use. We also acknowledge the Geographic and Cartographic Institute (Instituto Geográfico e Cartográfico – IGC) of São Paulo State for providing access to the DTM of the study area generated by EMPLASA. E.V.E.S. thanks CATALYST team for all support during the DTM extraction procedure. Lastly, E.V.E.S. thanks Leandro de Souza Novo, Sergio A. Barbosa, Eduardo Z. Molinez, Danilo Aparecido Rodrigues, Junior Martins dos Santos, and Jackson Martins dos Santos for all the support provided during the field survey activities.

Author's Contribution

Conceptualization, E.V.E.S. and C.M.A.; methodology, E.V.E.S and C.M.A.; fieldwork, E.V.E.S. and J.V.R.G.; software, E.V.E.S., R.M.C., C.M.A. and C.G.O.; validation, E.V.E.S.; formal analysis, E.V.E.S. and C.M.A.; investigation, E.V.E.S. and C.M.A.; data curation, E.V.E.S. and C.M.A.; writing—original draft preparation, E.V.E.S.; writing—review and editing, E.V.E.S. and C.M.A.; visualization, E.V.E.S. and C.M.A.; supervision, C.M.A.; project administration, C.M.A.; funding acquisition, E.V.E.S. and C.M.A. All authors have read and agreed to the published version of the manuscript.

Conflicts of Interest

The authors have no conflicts of interest to declare. The funders did not interfere in the development of the study, in the analysis or interpretation of the data, in the writing of the manuscript, or in the decision to publish the results.

References

AGUILAR, M. A.; NEMMAOUI, A.; AGUILAR, F. J.; QIN, R. Quality assessment of digital surface models extracted from WorldView-2 and WorldView-3 stereo pairs over different land covers. **GIScience & Remote Sensing**, v. 56, n. 1, p. 109–129, 2019. DOI: 10.1080/15481603.2018.1494408.

BECK, H. E.; ZIMMERMANN, N. E.; MCVICAR, T. R.; et al. Present and future Köppen-Geiger climate classification maps at 1-km resolution. **Scientific Data**, v. 5, n. 1, p. 180214, 2018. DOI: 10.1038/sdata.2018.214.

CARVALHO, R. M.; ALMEIDA, C. M. DE; ESCOBAR-SILVA, E. V.; ALVES, R. B. DE O.; LACERDA, C. S. DOS A. Simulation and Prediction of Urban Land Use Change Using 2 Markov Chain and Bayesian Inference by Means of Random 3 Change Allocation Algorithms. **Remote Sensing**, 2022. DOI: 10.3390/rs15010090.

CINTRA, J. P.; NERO, M. A.; RODRIGUES, D. GNSS/NTRIP service and technique: accuracy tests. **Boletim de Ciências Geodésicas**, v. 17, n. 2, p. 257–271, 2011. DOI: 10.1590/S1982-21702011000200006.

CLIMATE-DATA.ORG. Climate São Caetano do Sul. Available at <https://en.climate-data.org/south-america/brazil/sao-paulo/sao-caetano-do-sul-9603/>. Accessed on 31 Jan. 2023.

CRONEBORG, L.; SAITO, K.; MATERA, M.; MCKEOWN, D.; VAN AARDT, J. **Digital Elevation Models**. World Bank, Washington, DC, 2020.

ESA. About WorldView-2. Available at <https://www.eoportal.org/satellite-missions/worldview-2>. Accessed on 15 Aug. 2022.

FEWTRELL, T. J.; DUNCAN, A.; SAMPSON, C. C.; NEAL, J. C.; BATES, P. D. Benchmarking urban flood models of varying complexity and scale using high resolution terrestrial LiDAR data. **Physics and Chemistry of the Earth, Parts A/B/C**, v. 36, n. 7–8, p. 281–291, 2011. DOI: 10.1016/j.pce.2010.12.011.

FISHER, P. F.; TATE, N. J. Causes and consequences of error in digital elevation models. **Progress in Physical Geography: Earth and Environment**, v. 30, n. 4, p. 467–489, 2006. DOI: 10.1191/0309133306pp4.

FU, C. Y.; TSAY, J. R. STATISTIC TESTS AIDED MULTI-SOURCE DEM FUSION. **ISPRS - International Archives of the Photogrammetry, Remote Sensing and Spatial Information Sciences**, v. XLI-B6, p. 227–233, 2016.

GAMBA, P.; DELL ACQUA, F.; HOUSHMAND, B. SRTM data characterization in urban areas. **International Archives of Photogrammetry Remote Sensing and Spatial Information Sciences**, v. 34, n. (3/B), p. 55–58, 2002.

GROHMANN, C. H. Effects of spatial resolution on slope and aspect derivation for regional-scale analysis. **Computers & Geosciences**, v. 77, p. 111–117, 2015.

GUTH, P. L.; VAN NIEKERK, A.; GROHMANN, C. H.; et al. Digital elevation models: Terminology and definitions. **Remote Sensing**, v. 13, n. 18, p. 1–19, 2021. DOI: 10.1016/j.cageo.2015.02.003.

HENGL, T.; EVANS, I. S. Chapter 2 Mathematical and Digital Models of the Land Surface. p.31–63, 2009. DOI: 10.1016/S0166-2481(08)00002-0.

HUISING, E. J.; GOMES PEREIRA, L. M. Errors and accuracy estimates of laser data acquired by various laser scanning systems for topographic applications. **ISPRS Journal of Photogrammetry and Remote Sensing**, v. 53, n. 5, p. 245–261, 1998. DOI: 10.1016/S0924-2716(98)00013-6.

IBGE, Instituto Brasileiro de Geografia e Estatística. **Gross Internal Product of the Brazil's municipalities 2018 ('Produto interno bruto dos municípios 2018')**. Rio de Janeiro: Coordenação de Contas Nacionais, 2020. Available at <https://www.ibge.gov.br/estatisticas/economicas/contas-nacionais/9088-produto-interno-bruto-dos-municipios.html>. Accessed on 12 Feb. 2023.

IBGE, Instituto Brasileiro de Geografia e Estatística. Cities and states ('Cidades e estados'): São Caetano do Sul, 2023. Available at <https://cidades.ibge.gov.br/brasil/sp/sao-caetano-do-sul/panorama>. Accessed on 12 Feb. 2023.

ICS. Sustainable Cities Development Index: Brazil ('Índice de Desenvolvimento Sustentável das Cidades: Brasil'), 2022. ICS - Instituto Cidades Sustentáveis (Institute Sustainable Cities). Available at <https://idsc.cidadessustentaveis.org.br/rankings>. Accessed on 31 Jan. 2023.

LIU, Y.; BATES, P. D.; NEAL, J. C.; YAMAZAKI, D. Bare-Earth DEM Generation in Urban Areas for Flood Inundation Simulation Using Global Digital Elevation Models. **Water Resources Research**, v. 57, n. 4, 2021. DOI: 10.1029/2020WR028516.

MAUNE, D. F.; HEIDEMANN, H. K.; KOPP, S. M.; CRAWFORD, C. A. Introduction to DEMs. In: D. F.

Maune; A. Nayegandhi (Orgs.); **Digital elevation model. Technologies and applications: The DEM user's manual**. 3rd edition ed., 2018.

MESA-MINGORANCE, J. L.; ARIZA-LÓPEZ, F. J. Accuracy Assessment of Digital Elevation Models (DEMs): A Critical Review of Practices of the Past Three Decades. **Remote Sensing**, v. 12, n. 16, p. 2630, 2020. DOI: 10.3390/rs12162630.

MUGNIER, C.; FÖRSTNER, W.; WROBEL, B.; PADERES, F.; MUNJY, R. The Mathematics of Photogrammetry. In: J. C. McGlone (Org.); **Manual of photogrammetry**. 6th ed ed., 2013. American Society for Photogrammetry and Remote Sensing (ASPRS).

NASA. U.S. Releases Enhanced Shuttle Land Elevation Data. Available at <https://www2.jpl.nasa.gov/srtm/>. Accessed on 8 Aug. 2022.

NEMMAOUI, A.; AGUILAR, F. J.; AGUILAR, M. A.; QIN, R. DSM and DTM generation from VHR satellite stereo imagery over plastic covered greenhouse areas. **Computers and Electronics in Agriculture**, v. 164, p. 104903, 2019. DOI: 10.1016/j.compag.2019.104903.

NOVOA, J.; CHOKMANI, K.; NIGEL, R.; DUFOUR, P. Quality assessment from a hydrological perspective of a digital elevation model derived from WorldView-2 remote sensing data. **Hydrological Sciences Journal**, v. 60, n. 2, p. 218–233, 2015. DOI: 10.1080/02626667.2013.875179.

ORLANDI, A. G.; CARVALHO JÚNIOR, O. A. DE; GUIMARÃES, R. F.; BIAS, E. S.; Corrêa, D. C.; GOMES, R. A. T.; Vertical accuracy assessment of the processed SRTM data for the Brazilian territory. **Boletim de Ciências Geodésicas**, v. 25, n. 4, 2019. DOI: 10.1590/s1982-21702019000400021.

PCI GEOMATICS. Catalyst Profession - User's Guide. Chapter 6: Generating digital elevation models. 2022. Ontario, Canada.

QIN, R. A critical analysis of satellite stereo pairs for digital surface model generation and a matching quality prediction model. **ISPRS Journal of Photogrammetry and Remote Sensing**, v. 154, p. 139–150, 2019. DOI: 10.1016/j.isprsjprs.2019.06.005.

RODRÍGUEZ, E.; MORRIS, C. S.; BELZ, J. E. A Global Assessment of the SRTM Performance. **Photogrammetric Engineering & Remote Sensing**, v. 72, n. 3, p. 249–260, 2006. DOI: 10.14358/PERS.72.3.249.

ROMANHOLI, M. P.; LEAL, C.; TELLES, S. S. DE S.; SANTOS, C. DOS; REDIVO, I. A. C. Mapping Analysis Report of State of São Paulo 1:25,000 (Relatório de Análise do Mapeamento do Estado de São Paulo 1:25.000). (R. Duarte, Org.), 2015. Instituto Geográfico e Cartográfico – IGC.

SEEGERS, B. N.; STUMPF, R. P.; SCHAEFFER, B. A.; LOFTIN, K. A.; WERDELL, P. J. Performance metrics for the assessment of satellite data products: an ocean color case study. **Optics Express**, v. 26, n. 6, p. 7404, 2018. DOI: 10.1364/OE.26.007404.

SHAKER, A.; YAN, W. Y.; EASA, S. Using Stereo Satellite Imagery for Topographic and Transportation Applications: An Accuracy Assessment. **GIScience & Remote Sensing**, v. 47, n. 3, p. 321–337, 2010. DOI: 10.2747/1548-1603.47.3.321.

SHORTRIDGE, A. Shuttle Radar Topography Mission Elevation Data Error and Its Relationship to Land Cover. **Cartography and Geographic Information Science**, v. 33, n. 1, p. 65–75, 2006. DOI: 10.1559/152304006777323172.

TEUNISSEN, P. J. G.; ODOLINSKI, R.; ODIJK, D. Instantaneous BeiDou+GPS RTK positioning with high cut-off elevation angles. **Journal of Geodesy**, v. 88, n. 4, p. 335–350, 2014. DOI: 10.1007/s00190-013-0686-4.

USGS, United States Geological Survey. **Standards for digital elevation models**. Reston, VA, 1986.

VILLASENOR ALVA, J. A.; ESTRADA, E. G. A Generalization of Shapiro–Wilk's Test for Multivariate Normality. **Communications in Statistics - Theory and Methods**, v. 38, n. 11, p. 1870–1883, 2009. DOI: 10.1080/03610920802474465.

WALTHER, B. A.; MOORE, J. L. The concepts of bias, precision and accuracy, and their use in testing the performance of species richness estimators, with a literature review of estimator performance. **Ecography**, v. 28, n. 6, p. 815–829, 2005. DOI: 10.1111/j.2005.0906-7590.04112.x.

WEATHERALL, P.; MARKS, K. M.; JAKOBSSON, M.; et al. A new digital bathymetric model of the

world's oceans. **Earth and Space Science**, v. 2, n. 8, p. 331–345, 2015. DOI: 10.1002/2015EA000107.

WECHSLER, S. P.; KROLL, C. N. Quantifying DEM Uncertainty and its Effect on Topographic Parameters. **Photogrammetric Engineering & Remote Sensing**, v. 72, n. 9, p. 1081–1090, 2006. DOI: 10.14358/PERS.72.9.1081.

WEYDAHL, D. J.; SAGSTUEN, J.; DICK, Ø. B.; RØNNING, H. SRTM DEM accuracy assessment over vegetated areas in Norway. **International Journal of Remote Sensing**, v. 28, n. 16, p. 3513–3527, 2007. DOI: 10.1080/01431160600993447.

WÖLFL, A.-C.; SNAITH, H.; AMIREBRAHIMI, S.; et al. Seafloor Mapping – The Challenge of a Truly Global Ocean Bathymetry. **Frontiers in Marine Science**, v. 6, n. 283, p. 16, 2019. DOI: 10.3389/fmars.2019.00283.

ZAZO, S.; MOLINA, J.-L.; RODRÍGUEZ-GONZÁLVEZ, P. Analysis of flood modeling through innovative geomatic methods. **Journal of Hydrology**, v. 524, p. 522–537, 2015. DOI 10.1016/j.jhydrol.2015.03.011.

ZHOU, Y.; PARSONS, B.; ELLIOTT, J. R.; BARISIN, I.; WALKER, R. T. Assessing the ability of Pleiades stereo imagery to determine height changes in earthquakes: A case study for the El Mayor-Cucapah epicentral area. **Journal of Geophysical Research: Solid Earth**, v. 120, n. 12, p. 8793–8808, 2015. DOI: 10.1002/2015JB012358.

Main author biography

Elton Vicente Escobar Silva was born in Terra Nova do Norte (MT), in 1988. He owns a Bachelor's degree in Environmental Sciences from the Federal University of São Paulo (2015) with an exchange program in Technologies for Prevention and Mitigation of Natural Disasters at the Universität Hamburg, Germany (2014/2015). He obtained a Master´s Degree in Environmental Sciences from the Federal University of São Carlos (2019), with an internship at the USDA-ARS Hydrology and Remote Sensing Laboratory in the USA. He is currently a PhD candidate in Remote Sensing in the field of urban flooding simulation at the Brazilian National Institute for Space Research (INPE).